Nuclear Inst. and Methods in Physics Research, A 884 (2018) 140–149

Contents lists available at ScienceDirect

Nuclear Inst. and Methods in Physics Research, A

journal homepage: www.elsevier.com/locate/nima

Improving isotopic identification with *INDRA* Silicon–CsI(*Tl*) telescopes

O. Lopez [a,*], M. Pârlog [a,b], B. Borderie [c], M.F. Rivet [c,1], G. Lehaut [a], G. Tabacaru [c,d], L. Tassan-got [c], P. Pawłowski [e], E. Bonnet [f], R. Bougault [a], A. Chbihi [f], D. Dell'Aquila [h,c], J.D. Frankland [f], E. Galichet [c,g], D. Gruyer [a,f], M. La Commara [h], N. Le Neindre [a], I. Lombardo [i,h], L. Manduci [j,1], P. Marini [f,k], J.C. Steckmeyer [a], G. Verde [c], E. Vient [a], J.P. Wieleczko [f], for the INDRA collaboration

[a] *Normandie Université, ENSICAEN, UNICAEN, CNRS/IN2P3, F-14000 Caen, France*
[b] *Horia Hulubei National Institute for R&D in Physics and Nuclear Engineering (IFIN-HH), P.O.BOX MG-6, RO-76900 Bucharest-Màgurele, Romania*
[c] *Institut de Physique Nucléaire, CNRS/IN2P3, Univ. Paris-Sud, Université Paris-Saclay, F-91406, Orsay cedex, France*
[d] *Cyclotron Institute, Texas A&M University, MS 3366 College Station, TX 77843, USA*
[e] *Institute of Nuclear Physics PAN, ul. Radzikowskiego 152, 31-342 Krakow, Poland*
[f] *GANIL, CEA-DSM/CNRS-IN2P3, B.P. 5027, F-14076 Caen cedex, France*
[g] *Conservatoire National des Arts et Métiers, F-75141 Paris Cedex 03, France*
[h] *Dipartimento di Scienze Fisiche e Sezione INFN, Università di Napoli "Federico II", I80126 Napoli, Italy*
[i] *INFN — Laboratori Nazionali del Sud, Via S. Sofia 62, 95125 Catania, Italy*
[j] *EAMEA, CC19 F-50115, Cherbourg-Octeville Cedex, France*
[k] *CEN Bordeaux-Gradignan, Le Haut-Vigneau, F-33175, Gradignan Cedex, France*

ARTICLE INFO

Keywords:
Charged particle detector
Silicon–Caesium Iodide telescope
Isotopic identification
Fermi energy

ABSTRACT

Profiting from previous works done with the *INDRA* multidetector on the description of the light response $\mathcal{L}$ of the CsI(*Tl*) crystals to different impinging nuclei, we propose an improved $\Delta E - \mathcal{L}$ identification-calibration procedure for Silicon–Caesium Iodide (Si–CsI) telescopes, namely an Advanced Mass Estimate (*AME*) method. *AME* is compared to the usual, simple visual analysis of the corresponding two-dimensional map of $\Delta E - E$ type, by using *INDRA* experimental data from nuclear reactions induced by heavy ions in the Fermi energy regime. We show that the capability of such telescopes to identify both the atomic Z and the mass A numbers of light and heavy reaction products, can be quantitatively improved thanks to the proposed approach. This conclusion opens new possibilities to use *INDRA* for studying these reactions especially with radioactive beams. Indeed, the determination of the mass for charged reaction products becomes of paramount importance to shed light on the role of the isospin degree of freedom in the nuclear equation of state [1,2].

1. Introduction

One of the present motivations for investigating heavy-ion collisions at intermediate energies consists of improving our understanding of the equation of state for nuclear matter with the isospin degree of freedom. The advent of new accelerators, as SPIRAL2 at GANIL, SPES at LNL-Legnaro, FAIR at GSI, FRIB at MSU-NSCL, RIBF at Riken, FRIBS at LNS-Catania, providing high intensity radioactive beams, will cover a broad range of isospin (N/Z) ratios; here N and Z are the neutron and atomic numbers, respectively . Many products – different in terms of energy, charge and mass – emerge from these heavy ion reactions. If the measure of the kinetic energy and the atomic number have become usual nowadays, the exact mass and even the atomic mass number A are still difficult to determine, especially when they concern a wide range of elements of low or intermediate energy emitted in the whole space. Inventories of the techniques used for isotopic identification [3] put in evidence the pioneer works in the domains of: (i) the spectrometers [3,4] deflecting the charged particles in magnetic and electric fields, according to their identity; (ii) the time of flight, with pulsed beams, initially developed to measure the neutron velocity [3,5]; (iii) the telescope $\Delta E - E$ [3,6] - based on the specific energy loss in the first, thin stage for a given residual energy deposited in the second, thicker stage; (iv) the

* Corresponding author.
E-mail address: lopezo@in2p3.fr (O. Lopez).
[1] Deceased.

https://doi.org/10.1016/j.nima.2017.12.041
Received 28 July 2017; Received in revised form 12 December 2017; Accepted 12 December 2017
Available online 16 December 2017
0168-9002/

pulse shape discrimination in organic scintillators [7] for the neutron-gamma discrimination or in inorganic ones, as e.g. the caesium iodide [8], to identify light charged particles. Each of these items has some advantages but some drawbacks too. The present paper treats on the telescope technique – historically limited by the energy straggling [3,9], mainly at the crossing of the thin stage by the detected ion – but the most convenient from the volume and cost point of view, indeed. The evolution of these techniques have led to arrays which combine them according to the reaction types. Many magnetic spectrometers [10–12] as well as neutron walls [10,13,14] or 4π facilities for charged reaction products [10,15,16] have appeared. A review on the second and third-generation of multidetectors was done in the framework of the World Consensus Initiative (WCI) [10]. An experimental setup for studies of Reactions with Relativistic Radioactive Beams (R3B) is also under construction as part of the forthcoming Facility for Antiproton and Ion Research (FAIR) in Europe [17,18]. Jointly, new detection arrays like FAZIA [19,20], which fully exploit pulse shape analysis from silicon detectors for the nuclear fragment identification, are under construction to benefit from these future possibilities. Information on the isospin dependence of the nuclear *EOS* can then be obtained by properly choosing projectile–target colliding systems. To improve the present experimental capabilities in this framework, fast and reliable methods have been developed to assign Z and A of the detected charged reaction products when large numbers of $\Delta E - E$ telescopes were used [21–23] as it is the case, for example, for the CHIMERA array [24,25]. We present in this article the Advanced Mass Estimate (*AME*), a new approach, based upon the telescope technique for *INDRA* Silicon–CsI telescopes [26]. This approach will extend the isotopic identification to nuclear reaction products heavier than those commonly identified with standard $\Delta E - \mathcal{L}$ two-dimensional correlations. Here, ΔE indicates the energy lost in the 1st Silicon stage (Si) of the telescope and $\mathcal{L}$ the scintillation light produced in the 2nd stage, made by a CsI(Tl) scintillator crystal read by a photomultiplier and corresponds to the residual energy $E = E_0$ deposited by energetic charged reaction products. The main difficulties for identifying the mass number over a broad range of elements are related to the non-linear energy response of each of the two stages and, in particular, of the scintillator. Actually, the light response of the scintillator strongly depends on the reaction product identity (charge and mass), which makes difficult even the determination of the deposited energy. At present time, the isotopic identification is visually achieved only for light nuclei from hydrogen up to (roughly) carbon isotopes for most of the *INDRA* Si–CsI telescopes. For some specific telescopes with smaller thickness - 150 μm instead of 300 μm -, an increased gain has been used in order to improve the energy resolution and hence the isotopic separation during the 5th *INDRA* campaign performed at *GANIL* a few years ago. In doing so, the isotopic identification for these specific telescopes has been slightly augmented up to oxygen isotopes for the best cases. This is also the case for the CHIMERA silicon–caesium iodide telescopes [24] and the cited paper is a nice piece of work in the field, employing – for the identification of nuclear fragments – the automatic procedure developed in the Ref. [23]. By exploiting a functional based on Bethe formula [27] for the stopping power, which leads to a direct algebraic relation – depending on seven parameters – between the measured quantities ΔE and E in the corresponding two dimensional plane, this method succeeds to reproduce the mass distribution (integrated over the energy) in the range $Z = 2 - 8$ considered and even to a reasonable extrapolation for all $Z \leq 12$. The approach in the present paper is different. By considering the specific energy loss of all detected nuclear fragments [28–31], it uses precise calibrations of the measured quantities: the answer of the first, silicon stage of a telescope and the light induced in the last one — the caesium iodide scintillator, respectively. Their separate descriptions take into account the evolution of the charge carriers generated in each detector by the passing fragment, without worrying about a mathematical connection between the two responses. We will put thus in evidence the sensitivity of the scintillation, and consequently, of the whole telescope, to the mass of the impinging ejectile, and that even for very heavy fragments, up to the projectile (here $Z = 54$).

To improve and optimize information coming from *INDRA* Si–CsI telescopes as far as the mass number is concerned, we started from the pioneer works of Pârlog et al. [32,33] which provide an accurate physical description of the light response produced by the CsI(*Tl*) crystals. In these articles, two formulas have been derived concerning the relation between the light signal $\mathcal{L}$, the atomic number Z, the mass number A and the incident energy E_0 of a reaction product detected by a CsI scintillator. The proposed method was then used and tested on data recorded with *INDRA* during the fifth campaign, with telescopes having as first stage 300 μm or 150 μm-thick Silicon detectors. These experimental data were obtained by bombarding ^{112,124}Sn targets with ^{124,136}Xe beams at 32A MeV and 45A MeV.

The paper is organized as follows. In Section 2, we recall the main results of references [32,33] concerning the role of quenching and knock-on electrons in scintillation light from the CsI(*Tl*) crystals and show the quality of the analytical description. Section 3 describes the Advanced Mass Estimate (*AME*) method and the comparisons with standard *INDRA* isotopic identification. In Section 4, determination and uncertainty on A are discussed. In Section 5, we present a summary of this work.

2. Quenching and knock-on electrons (δ-rays) in scintillation light of CsI(*Tl*) crystals

Caesium iodide scintillators, CsI(*Tl*), doped with thallium at a level of 0,02–0,2% molar concentration, are inorganic crystals where the scintillation light is produced by the activation (excitation) of the thallium atoms encountered by the carriers (electrons and holes) produced during the motion of the incoming charged product. The activation results in an emission of light by the excited thallium atoms in the green band at 550 nm. The differential scintillation light output $\frac{d\mathcal{L}}{dE}$ as a function of energy E is often described by means of the Birks formula [34]:

$$\frac{d\mathcal{L}}{dE} = \mathcal{S}\frac{1}{1 + \mathcal{KB}\left(\frac{dE}{dx}\right)}, \tag{1}$$

$\mathcal{S}$ being the scintillation efficiency and $\mathcal{KB}$ the quenching coefficient. The differential light decreases as the stopping power $\left(\frac{dE}{dx}\right)$ increases; this is the so-called quenching effect, more pronounced for the heavier ions leading to high carrier concentrations. Under the approximation $\left(\frac{dE}{dx}\right) \propto AZ^2/E$, the integral over the variable E of the above equation provides a simple formula for the total light response $\mathcal{L}$ [35] as a function of the initial energy E_0 of the detected ion:

$$\mathcal{L}(E_0) = \int_0^{E_0} \mathcal{L}(E)dE = a_1 E_0 \left[1 - a_2 \frac{AZ^2}{E_0} \ln\left(1 + \frac{1}{a_2 AZ^2/E_0}\right)\right], \tag{2}$$

The gain coefficient a_1 includes both the scintillation efficiency and the electronic chain contribution to the signal amplification. The quenching coefficient a_2 is mainly related to the prompt direct recombination of part of the electrons and holes, which thus are not participating to the excitation of the activator atoms.

The expressions (1) and (2) were used, with reasonable results [34–36] in the case of light charged particles or Intermediate Mass Fragments (IMFs) of rather low energy per nucleon E/A, *i.e.* as long as the contribution to the light response of the knock-on electrons or δ-rays, escaping the fiducial volume of very high carrier concentration close to the trajectory of the particle/ion, remains insignificant. Actually, above a certain energy per nucleon threshold $e_\delta = E_\delta/A$, the incident particle/ion starts to generate these rapid electrons, which are characterized by a small stopping power. Consequently, the fraction $\mathcal{F}(E)$ - firstly introduced by Meyer and Murray [37] -, of the energy dE deposited into a slice dx and carried off by the knock-on electrons is practically not affected by quenching. The δ-rays increase thus the light output and this should be necessarily taken into account at energies higher than a few MeV/nucleon, especially for heavier ions.

As it penetrates into a CsI crystal, an energetic charged particle/ion is gradually losing its energy (from E_0 to 0) mainly by ionization – the electronic stopping power –, leading to the scintillation, but also, in a smaller extent, by interacting with the host lattice nuclei – the nuclear stopping power –, lost for the radiative transitions. Both stopping powers can be quantitatively predicted, *e.g.* by using Ziegler tables [28] appealing to the work of Lindhard et al. [29]. Within the *INDRA* collaboration, we use stopping power tables for heavy ions in solids from Northcliffe and Schilling at low energies [30] and from Hubert and Bimbot at high energies [31], both matched at 2.5 MeV/nucleon. They provide quite accurate results in the low and intermediate energy range, *i.e.* from few hundreds of keV/nucleon up to 100 MeV/nucleon, of interest here. More than a decade ago, Pârlog et al. [32,33] put in evidence the role of the two types of energy loss to the quenching and also found the dependence of the fraction $\mathcal{F}(E)$ on the instantaneous velocity (or energy per nucleon E/A). They disentangled the contributions of the carriers produced in the main particle track and of the δ-rays to the scintillation too. The authors quantified these processes in a simple Recombination and Nuclear Quenching Model ($RNQM$) connecting the exact value of the total emitted light $\mathcal{L}$ to both the electronic and nuclear infinitesimal stopping powers along the incident particle track via numerical integration [32]. The model contains Eq. (1) as a particular case. Under well argued approximations, they derived a more friendly analytical formula relating $\mathcal{L}$ to the quantities Z, A and E_0 [33]:

$$\mathcal{L}(E_0) = a_1 E_0 \left[1 - a_2 \frac{AZ^2}{E_0} \ln\left(1 + \frac{1}{a_2 AZ^2/E_0}\right) + a_2 a_4 \frac{AZ^2}{E_0} \ln\left(\frac{E_0 + a_2 AZ^2}{a_3 A + a_2 AZ^2}\right)\right], \quad (3)$$

for an incident energy E_0 in the CsI(Tl) higher than the threshold E_δ at which the δ-rays start to be generated. Besides the coefficients a_1, a_2, with the same physical signification as above in Eq. (2), two others appear: the energy per nucleon $a_3 = e_\delta = E_\delta/A$, (a few MeV/nucleon) and $a_4 = \mathcal{F}$ – the fraction (a few tenths of percents) of energy – they are carrying off, taken as a constant irrespective of current energy E along the particle path above E_δ. At low energy ($E \leq E_\delta$), $\mathcal{F} = 0$ and only the first term is present, then Eq. (3) is reduced to Eq. (2). These four parameters have then to be evaluated by using a number of suitable calibration points by a fit procedure.

The relation (3) is purely analytical and can then be easily implemented for calibration purpose. It is less accurate than the exact treatment provided in $RNQM$ [32] especially at low energy. One drawback is also the step function used for $\mathcal{F}(\mathcal{E})$, which jumps from 0 to a_4 at $E = E_\delta$ in order to allow the analytical integration over E. This introduces a discontinuity in the function $\mathcal{L}(E)$ at this connection point, especially for very heavy fragments [33]. Nevertheless, it may be *ad hoc* improved by slightly improving the continuity of the fraction $\mathcal{F}(E)$ around E_δ. In this work, we consider that the use of the analytical expression will only marginally affect the results, taking into account the intrinsic quality of the Silicon wafers and of the CsI crystals of the *INDRA* telescopes, which does not secure the precision required to appreciate such discrepancies. Moreover, the total light $\mathcal{L}$ emitted by the CsI(Tl) scintillators is not directly measured, but reconstructed, through the procedure described by Pârlog et al. [33], starting from two components of the scintillation light measured by integrating the signal in the fast and slow time gates [33]. Nevertheless, for a more rigorous and accurate treatment, the use of the exact formulation of $RNQM$ [32] is preferable when possible, for example with high-quality detectors such as *FAZIA* Si–CsI telescopes. This will be the subject of a forthcoming paper.

As an example of the quality attained with our analytical description for the scintillation light in CsI(Tl) crystal, Fig. 1 displays the energy–light correlation $E_0 - \mathcal{L}$ using Eq. (3) superimposed on *INDRA* data concerning the system ^{136}Xe + ^{124}Sn at 32A MeV, for a specific Si–CsI telescope.

Each full/coloured line in Fig. 1 corresponds to a given nucleus with an atomic number Z and a mass number A. We have chosen here to display isotopic lines with $A = 2Z+1$ for even-Z nuclei. We will see in the following that this mass assumption is quite reasonable for IMFs when considering the neutron (n)-rich system ^{136}Xe+^{124}Sn. For a given energy E_0 - determined as shown in the next section -, the heavier the nucleus, the smaller the light value $\mathcal{L}$ is; this is a direct consequence of the ratio nuclear/electronic stopping powers, and also of the quenching effect. Both quantities increase with the charge and the mass of the fragment and decrease when E_0 increases. Additionally, above a certain velocity, δ-electrons are generated, very efficient for light production. These are the reasons why the curvature of the different isotopic curves shown in Fig. 1 evolves towards a linear behaviour at higher light/energy, here $\mathcal{L} > 600$. It is worthwhile to mention that the δ-rays contribution to the light is quite large, reaching 20 – 50% for $Z > 20$, as pointed out in Ref. [33] and must be definitely included in order to reproduce the experimental data. To obtain the results displayed in Fig. 1, we have used calibration points coming from secondary light beams stopped in CsI detectors from $Z = 1$ up to $Z = 5$ together with punched through events in the Silicon layer when possible. In a two dimensional $\Delta E - \mathcal{L}$ plot, these points are close to the ordinate ΔE axis, *i.e.* to fragment energies slightly higher than that necessary to traverse the Silicon stage of the telescope and to reach the CsI(Tl) one with a quite small residual energy, sufficient however to be seen in the scintillator stage.

In order to better appreciate the performances concerning the isotopic identification in *INDRA* CsI telescopes, we display in Fig. 2 the correlation between the energy and the CsI light signal (same as for Fig. 1) for 4 selected elements (carbon, fluorine, magnesium and sulphur), and for systems with different neutron content: ^{124}Xe+^{112}Sn and ^{136}Xe+^{124}Sn at 32A MeV. We can observe a significative difference between the two systems concerning the neutron richness of the produced fragments (higher masses for the (n)-rich system in blue) as one could expect from simple physical arguments. It is worthwhile to mention that this result requires indeed a very good stability for the CsI light response. This is done in *INDRA* by monitoring a laser pulse all along the data taking [33]. Thus, Fig. 2 suggests that the CsI light signal can help to discriminate the different isotopes, here at least up to $Z = 16$ (sulphur). In the following, we will use this additional valuable information to improve the usual $\Delta E - \mathcal{L}$ identification method for heavier elements than typically done up to carbon or nitrogen.

To illustrate the overall sensitivity of the Si–CsI(Tl) telescopes to the mass number, Fig. 3 displays the $\Delta E - \mathcal{L}$ correlation bidimensional matrix of the 2nd module (including a 300 μm-thick Si) for the 1st ring ($2° \leq \theta \leq 3°$) of *INDRA*, and for ^{124}Xe and ^{136}Xe projectiles on ^{124}Sn at 32A MeV and 45A MeV bombarding energies. The bright/yellow spots, indicated by arrows on the borders of the geometrical loci for $Z = 54$ (two in the region of the 32A MeV incident energy and other two in that of 45A MeV one) correspond in both cases to the (n)-poor or (n)-rich projectiles, respectively. These findings indeed show the good sensitivity of the response of *INDRA* telescopes to the mass of the detected ejectile, thus calling for a deeper analysis of the experimental data as presented hereafter.

3. Advanced mass estimate (*AME*) in *INDRA* Si–CsI telescopes

In this section, we are going to present the new *AME* identification method in details. We use information given by the energy lost in the Silicon detector, ΔE, and the atomic number Z taken from the usual $\Delta E - \mathcal{L}$ identification method in a Si–CsI map (see Fig. 3 for example). Doing so, we benefit from the previous identification works done for *INDRA* data : Z identification in Si–CsI matrices by semi-automatic [23] or handmade grids and the careful calibration of the Silicon detector, by means of α particle source and secondary beams stopped in this layer [38]. For heavy ions ($Z > 15$), the Pulse Height Defect (PHD) in this detector can be large [38] and has to be carefully evaluated. For *INDRA*, we use the elastic scattering of low-energy heavy ion beams (Ni and Ta at 6 AMeV) which are stopped in Silicon detectors. Traditionally, we quantify the PHD as a function of the atomic number, the energy

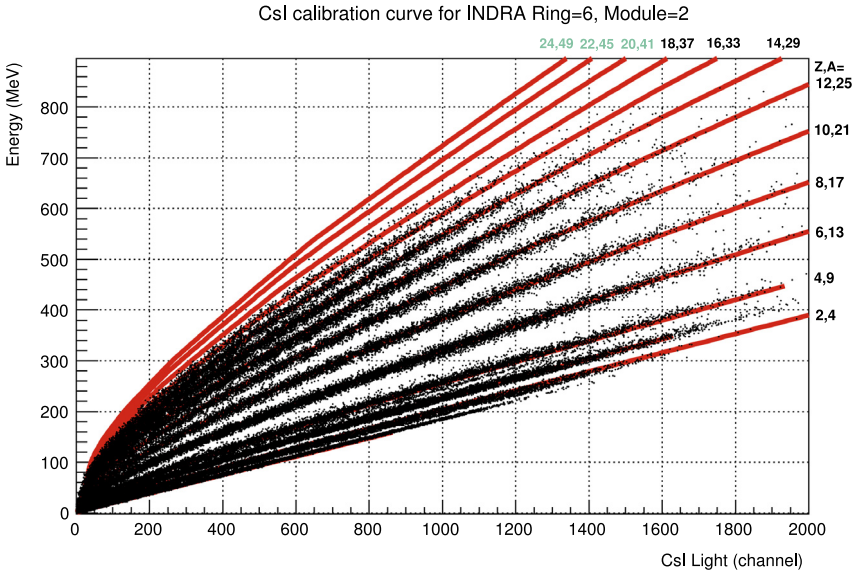

Fig. 1. Energy (E_0)–Light ($\mathcal{L}$) correlation in a CsI(Tl) scintillator, for even-Z fragments. The points correspond to data from the telescope 2 of the ring 6 ($14° \leq \theta \leq 20°$) of the *INDRA* 4π array for the system ^{136}Xe + ^{124}Sn at 32A MeV. The atomic number of the heaviest fragments emitted in this angular domain is $Z = 16$. The full/coloured lines illustrate the Eq. (3) predictions. The mass number for each element is likely corresponding to the most probable isotope, here $A = 2Z + 1$. See text for explanation. (colour online).

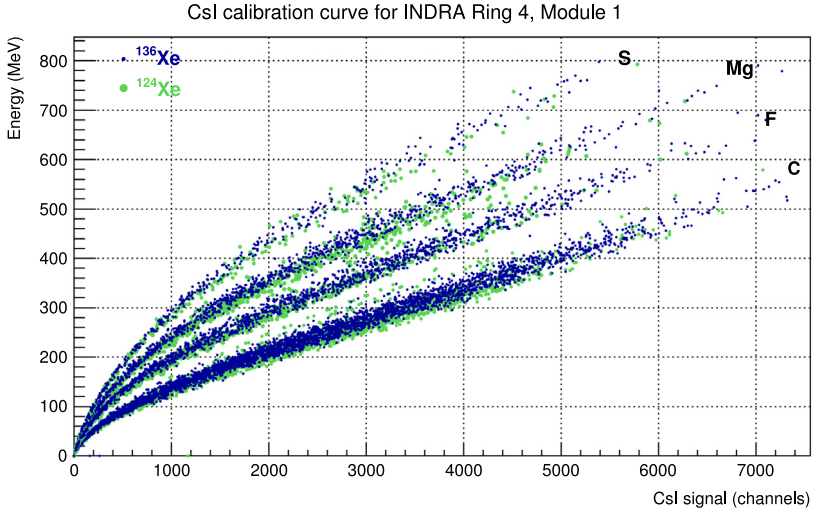

Fig. 2. Energy (E_0)–Light ($\mathcal{L}$) correlation in the CsI(Tl) scintillator of telescope 1 of the ring 4 ($7° \leq \theta \leq 10°$), shown here for the two systems ^{124}Xe + ^{112}Sn and ^{136}Xe + ^{124}Sn at 32A MeV, and for some selected elements: carbon, fluorine, magnesium and sulphur. The large/green symbols correspond to the (n)-poor system (^{124}Xe + ^{112}Sn) and the small/blue ones to the (n)-rich system (^{136}Xe + ^{124}Sn). (colour online).

of the particle and the quality of the detector, according to Moulton formula [39].

For a given element characterized by its atomic number Z, the measured energy ΔE deposited in the first layer of the Si–CsI(Tl) telescope depends on the velocity, or the initial energy and the mass of the incident particle and, in principle, it cannot provide by itself the two quantities without ambiguity. To perform consistently the isotopic identification in Si–CsI matrices, we then assume a starting value A_0 for the mass number concerning one detected nucleus with its atomic number Z and, by constraining the energy loss ΔE in the Silicon stage at the measured value, we compute both the total energy at the entrance of the Silicon stage and the residual energy E_0 deposited in the CsI(Tl) by using the above-mentioned range and energy loss tables [30,31]. This procedure imposes also to accurately evaluate the thickness of the ΔE Silicon detector. The value of the scintillation light $\mathcal{L}$ given by Eq. (3) for the residual energy value E_0 associated to this starting value of A is then compared to the experimental light output $\mathcal{L}_{exp}$ from the CsI(Tl). In order to determine the best 'theoretical' value $\mathcal{L}(E_0)$, we iterate on mass number A (and consequently on the value of E_0) until we find the best agreement between the theoretical and experimental values of the light, always compatible with the energy lost in the Silicon stage. It is worthwhile to mention that the mass number is an integer and, as such, is varied by increment of one mass unit. At the end of the iteration, we get an integer mass number, giving the best agreement for the experimentally determined quantities ΔE and $\mathcal{L}_{exp}$ as displayed in Fig. 3. This is the basis of the Advanced Mass Estimate (*AME*) method, which, by making use in a consistent way of the experimental quantities ΔE and $\mathcal{L}_{exp}$, brings a more accurate information on both the mass and the residual energy (and consequently the total energy too).

As one may guess from Fig. 3, the calibration for the Silicon detector should be as accurate as possible to perform the best isotopic identification. The formula given by [39] used to calculate the PHD does not depend on the ion mass. This is certainly an advantage as it simplifies our approach, but it may become a drawback too. Even if the calibration of the Silicon stage can be considered to be rather accurate, we estimate that it represents at present time one of the known limitations for the

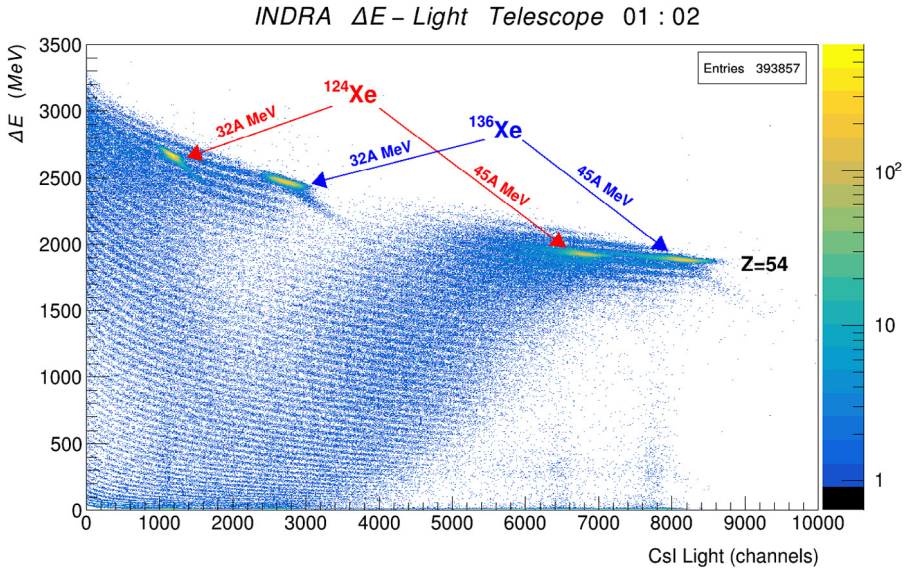

Fig. 3. $\Delta E - \mathcal{L}$ correlation for *INDRA* data obtained with a module placed at a forward angle for the ^{124,136}Xe + ^{124}Sn systems at 32A MeV and 45A MeV bombarding energies, illustrating its sensitivity to the detected fragment mass. The Silicon stage is 300 μm thick. See text for explanation. (colour online).

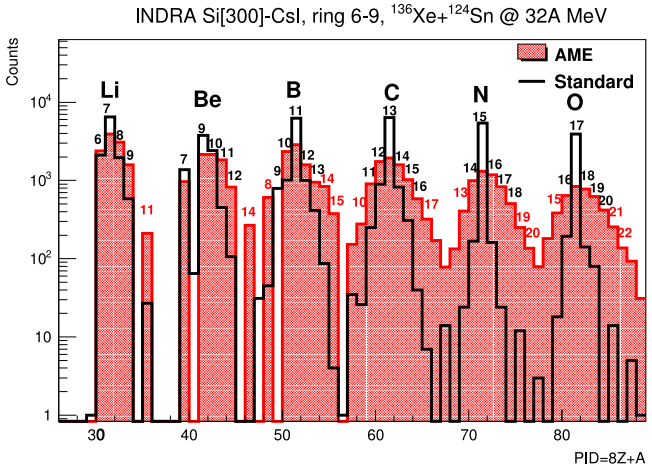

Fig. 4. Isotopic distributions from lithium (left) to oxygen (right). The isotopes are indicated by their mass numbers. The black and grey/red labels are explained in the text. Data concern the rings 6 to 9 for the system ^{136}Xe + ^{124}Sn system at 32A MeV recorded with *INDRA* and correspond to forward angles between 14° and 45° in laboratory frame. Empty histograms are the results obtained with the standard $\Delta E - \mathcal{L}$ method and filled histograms those from the *AME* method for the same sample of events. The Silicon stage is 300 μm thick. (For interpretation of the references to colour in this figure legend, the reader is referred to the web version of this article.)

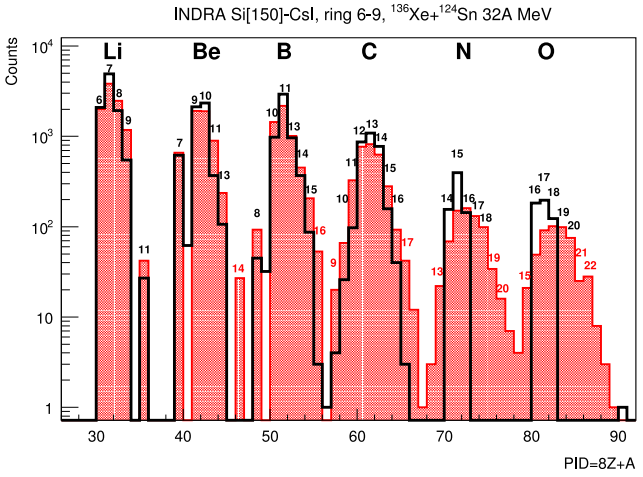

Fig. 5. Isotopic distributions from lithium (left) to oxygen (right). The isotopes are indicated by their mass numbers. The black and grey/red labels are explained in the text. Data concern the specific telescopes with a high gain 150 μm Silicon from rings 6 to 9 for the system ^{136}Xe + ^{124}Sn system at 32A MeV recorded with *INDRA* and correspond to forward angles between 14° and 45° in the laboratory frame. Empty histograms are the results obtained with the standard $\Delta E - \mathcal{L}$ method and filled histograms those from the *AME* method for the same sample of events. (For interpretation of the references to colour in this figure legend, the reader is referred to the web version of this article.)

extension of the identification method towards heavier nuclei ($Z > 30$). Nevertheless, we will see in the following that it does not hamper very much the isotopic identification for such heavy products.

In the next sections, we will estimate the performances of this new identification procedure. As a first step, we will benchmark the new method for light nuclei where isotopic identification is already achieved ($1 \leq Z \leq 6$–8) with traditional methods. In a second step, we will then get some quantitative values concerning the improvement for the isotopic identification of heavier nuclei, up to xenon isotopes in our case.

3.1. Benchmark with the standard $\Delta E - \mathcal{L}$ method

Using the *AME* method, we obtained isotopic distributions of light nuclei that have been compared to the ones obtained with the standard method (making use of visual grids) for *INDRA* Si–CsI telescopes. Fig. 4 displays the isotopic distributions obtained by the new *AME* method (filled histograms) and the standard $\Delta E - \mathcal{L}$ one, using standard grids (empty histograms), from lithium ($Z = 3$) up to oxygen ($Z = 8$) isotopes. The numbers indicate the isotope masses. For the meaning of the colours of these numbers : black or grey/red, see Section 4. The Particle IDentifier (PID) defined as $PID = 8Z + A$, and allowing to separately observe the neighbouring elements, was chosen as abscissa for this representation. The modules incorporating silicon detectors of only 300 μm thickness were kept for this representation. We observe an overall good agreement for the most probable isotopes, found as having the mass number $A = 2Z + 1$ as already discussed for Fig. 1.

We also notice that the new method can still provide isotopic identification for less abundant species ((n)-rich and (n)-poor carbon to oxygen isotopes for example) since it does not use any visual recognition to build the grids for which a sufficiently large production cross-section

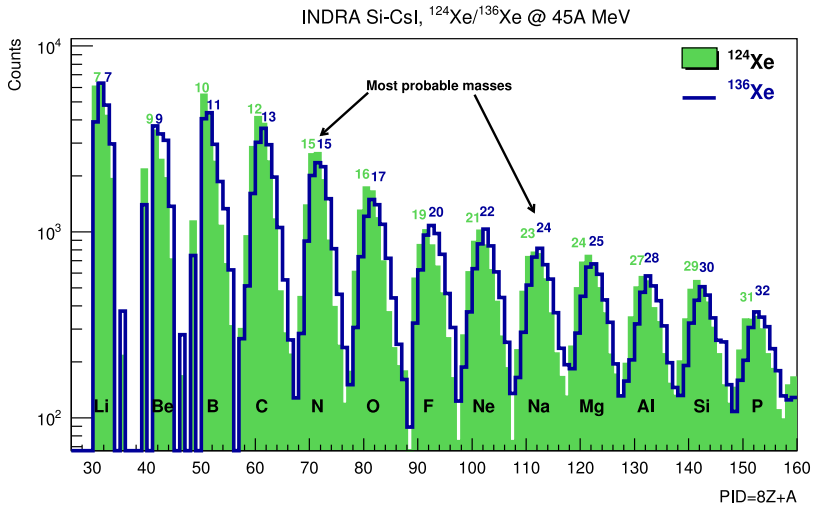

Fig. 6. Isotopic distributions (PID as $8Z + A$) from lithium (left) to phosphorus isotopes (right), provided by *AME* with ordinary telescopes (300 μm-thick Si). The filled histograms correspond to the ^{124}Xe + ^{112}Sn system and the empty histograms to the ^{136}Xe + ^{124}Sn system at the same incident energy per nucleon $E/A = 45\ MeV$ (*INDRA* data). The most abundant isotope in each case is indicated too. (colour online).

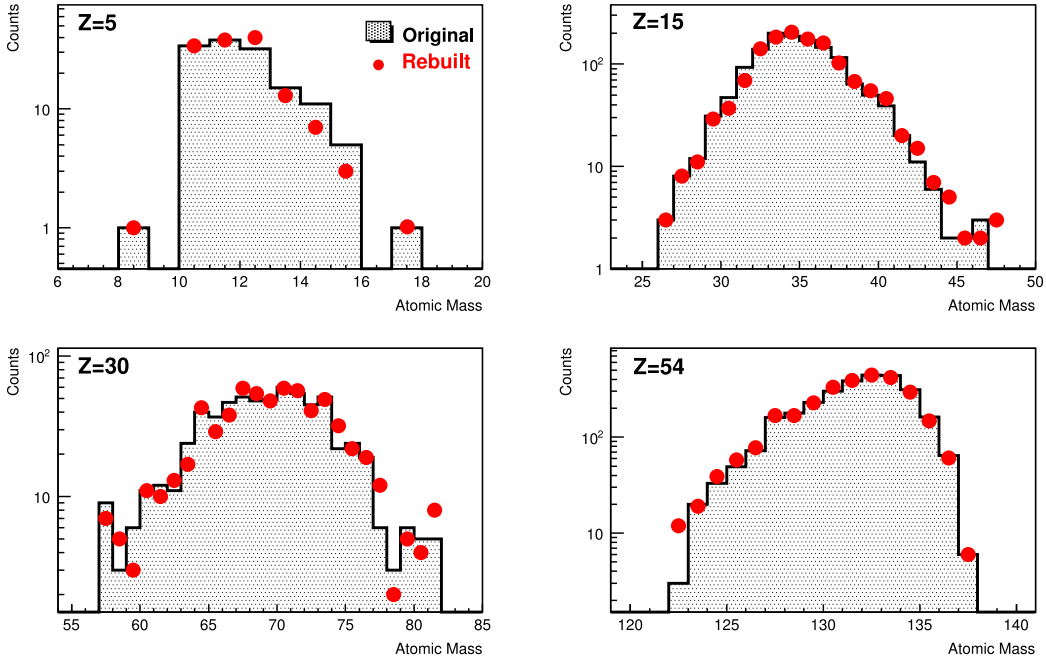

Fig. 7. Isotopic mass distributions for different elements from $Z = 5$ up to $Z = 54$ for the $^{136}Xe + ^{nat}Sn$ system at $32A$ MeV. The histograms display the original isotopic distributions and the symbols the rebuilt ones (colour online).

is needed. This is clearly an improvement compared to the standard methods since it allows to recover the overall isotopic distributions for a given element Z, at least in this range of atomic numbers $Z = 3$–8. This new feature is welcome for studying isospin effects as for example isotopic yields or isoscaling [2,40].

To complete the benchmark on light nuclei, we also present in Fig. 5 the isotopic distributions obtained for the specific 150 μm-thick Silicon detectors with a high gain, but for lower statistics. These ones allow to better discriminate the isotopes for light IMFs (up to $Z \approx 8$) and constitute a more stringent test for the comparison. Actually, the mass distribution for the carbon isotopes given by the standard method becomes now significantly larger, closer to that provided by the *AME* method, which recovers more exotic species. We also notice that even the yield for the most probable isotopes given by the two methods are sometimes not the same, due to the absence of grids for some telescopes where the visual inspection does not permit to define properly the isotopes curves and boundaries. This is particularly true for $Z = 7$–8. In Figs. 4 and 5, the black numbers indicate the masses estimated with an uncertainty lower than one mass unit, while the grey/red ones, those affected by higher uncertainty. This specific point is developed in Section 4.

3.2. Comparison with different isospin systems

To extend and confirm the previous results, we checked the isotopic identification by means of the *AME* method for two systems with different isospins : ^{124}Xe + ^{112}Sn and ^{136}Xe + ^{124}Sn at the same incident energy per nucleon of 45 AMeV without any event selection except here a common trigger multiplicity $M = 1$. These latter are also part of the data extracted from the 5th *INDRA* campaign performed at GANIL. We could reasonably expect an overproduction of (n)-rich isotopes in the case of the (n)-rich ^{136}Xe + ^{124}Sn system, for light nuclear fragments. In

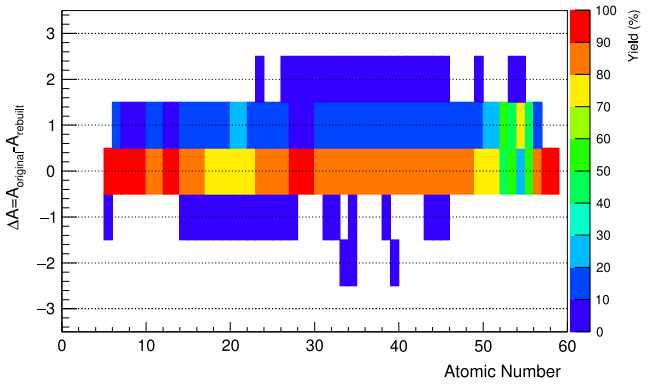

Fig. 8. Correlation between the mass difference ΔA and the atomic number Z. The weights of each bin in atomic number Z have been normalized to 100% (colour online).

the following, we compared the isotopic distributions obtained for both systems, in order to see whether we observe any difference reflecting the possible different production yields for a given element Z.

Fig. 6 shows the isotopic distributions from lithium to phosphorus isotopes, provided by Silicon–CsI telescopes. We display here only the results for the 300 μm-thick Silicon ones. We can observe a global shift of the isotopic distribution towards more (n)-rich species for the (n)-rich system (^{136}Xe + ^{124}Sn) as compared to the (n)-poor one (^{124}Xe + ^{112}Sn). If we consider the most abundant isotope per element, it is ^{7}Li instead of ^{6}Li and ^{17}O instead of ^{16}O for example, together with the enhancement of very (n)-rich isotopes production for the (n)-rich system (^{136}Xe + ^{124}Sn) as one could expect. This illustrates the fact that the isotopic distributions determined with AME are not an artefact of the method but they truly could be associated to the genuine (physical) isotopic distributions.

4. Qualifying the isotopic identification

4.1. Sensitivity analysis

In order to check the sensitivity of the new *AME* method, we follow the same spirit as presented in [24]. We evaluate the robustness of the isotopic identification obtained with *AME* by degrading intentionally the energy resolution of the silicon and CsI detectors and see the results on the rebuilt mass $A_{rebuilt}$. We take some realistic values for the energy resolution for the silicon detectors and CsI light output coming from [24,33], here 2% for the silicon and 4% for the CsI. As original values for this test, we take the experimental data in term of mass $A_{original}$, and the well defined spectrum for the total energy $E_{tot} = \Delta E + E$. Starting from E_{tot}, we compute the energy lost in the silicon layer thanks to the energy loss tables and we degrade it by applying a finite energy resolution of 2% to get the quantity $\Delta E'$. We then compute the corresponding residual energy E' which takes into account the silicon energy uncertainty. From E', we are able to determine the light $\mathcal{L}'$ in the CsI using Eq. (3). Applying a finite resolution of 4% for the light in the CsI, we get now the quantity $\mathcal{L}''$. We can then redo the *AME* procedure from the new $\Delta E'$ and $\mathcal{L}''$ in order to determine a computed mass $A_{rebuilt}$ to be compared to the original one $A_{original}$. Doing so, we can check our isotopic determination with the *AME* method against realistic energy ΔE and light $\mathcal{L}$ uncertainties, these latter including also the uncertainties coming from the energy loss tables calculations. The results from $Z = 5$ up to the projectile atomic number, here $Z = 54$, are displayed in Fig. 7 where the original isotopic distributions and the rebuilt ones are presented for the ^{136}Xe + ^{nat}Sn system at 32A MeV. Even though some discrepancies appear here and there in the cases with very poor statistics, we can notice a very good global agreement for all elements. This gives a certain credit concerning the robustness of the *AME* method.

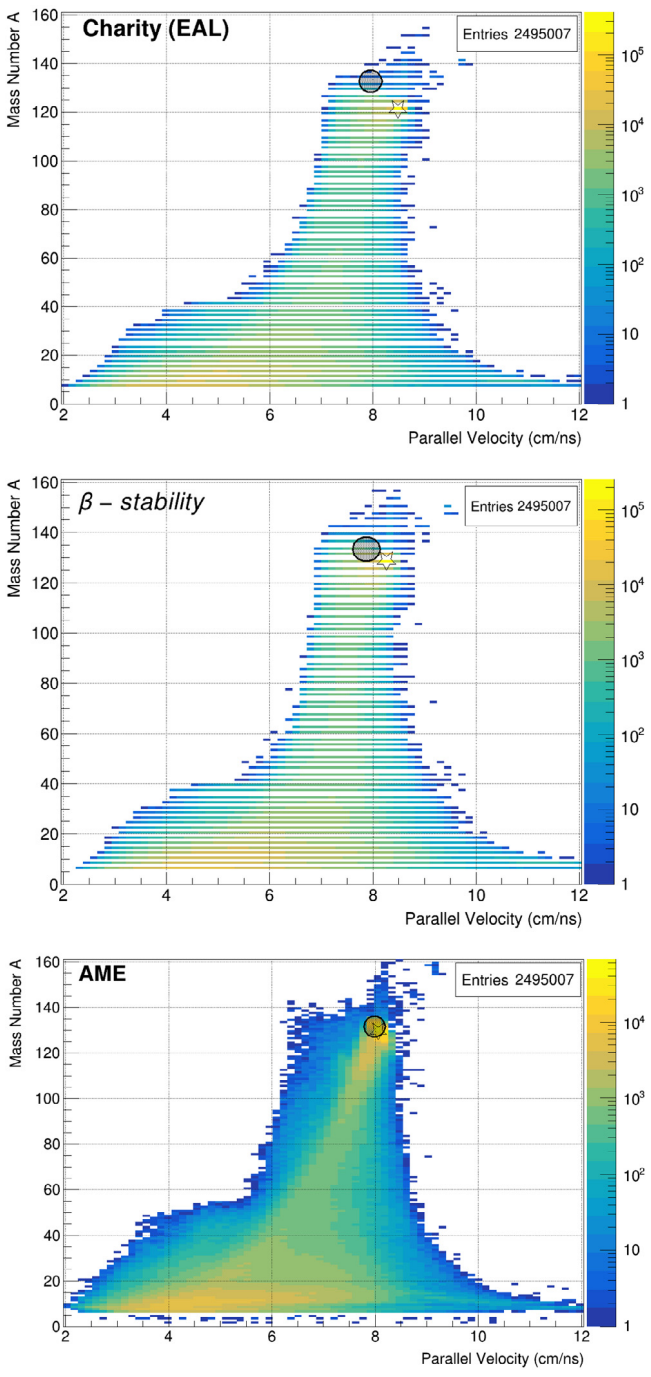

Fig. 9. *INDRA* data. Correlation between the velocity V_z in cm/ns, parallel to the beam direction, and the atomic mass A for ^{136}Xe + ^{112}Sn at 32A MeV obtained in the very forward rings (1–5) for a trigger multiplicity $M \geq 1$. The upper panel displays the traditional $\Delta E - \mathcal{L}$ identification method with no mass determination and the EAL hypothesis for the masses of the fragments. The same for the middle panel, but with the β-stability valley hypothesis for the masses of the fragments. In the lower panel are plotted the results obtained with the new *AME* method. The circles indicate the projectile mass ($A = 136$) and the parallel projectile velocity ($V_z = 7.9$ cm/ns), while the stars correspond to the peak of each two-dimensional distribution. (colour online).

To get a more global picture about this finding, we present in Fig. 8 the difference ΔA between the original mass $A_{original}$ and the rebuilt one $A_{rebuilt}$ as a function of the atomic number Z, always for the ^{136}Xe + ^{nat}Sn system at 32A MeV. The weights of each bin in atomic number Z have been normalized to 100% in order to give directly the percentages associated with ΔA for a given element Z. In almost all cases, we obtain

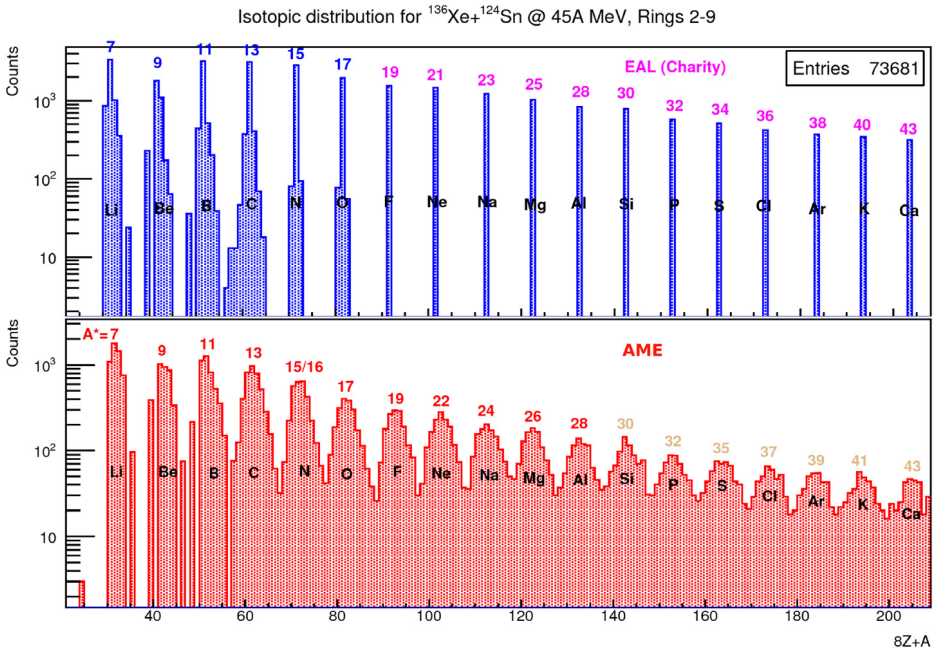

Fig. 10. *INDRA* data. Particle IDentification $PID = 8Z + A$ for the ^{136}Xe + ^{112}Sn at 32A MeV obtained in the forward rings (1–5) for a trigger multiplicity $M \geq 1$. The upper panel refers to the standard method: above $Z = 8$, there is no isotopic identification and a mass hypothesis (here EAL [41]) is necessary. The lower panel illustrates the new *AME* method, leading – for each element – to their distribution of isotopes, the most abundant ones being indicated by their mass numbers. The grey numbers correspond to elements where $\delta A > 0.5$ (see text for details). (colour online).

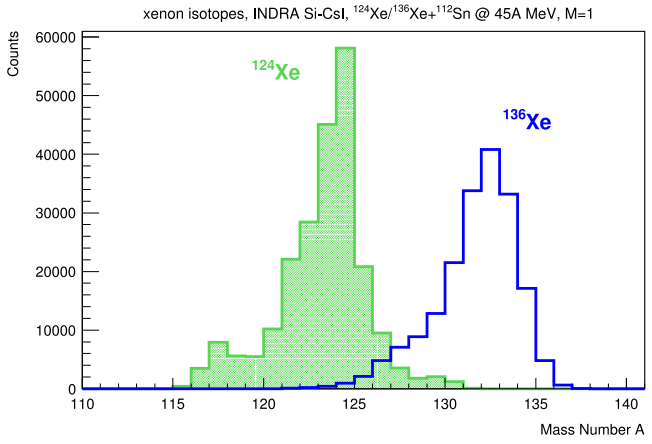

Fig. 11. *INDRA data.* Isotopic distribution of xenon isotopes ($Z = 54$) for the ^{124}Xe + ^{112}Sn (filled histogram) and ^{136}Xe + ^{112}Sn (empty histogram) at 45A MeV provided by the *AME* method, in the most forward rings (1–3) for a trigger multiplicity $M = 1$. (colour online).

ΔA values centred around 0 for the largest percentage values, with 75–80% in average, even 85–90% for $Z = 5$–12. In brief, we can conclude from Fig. 8 that ΔA variation is negligible for $Z = 5$–12, does not exceed ± 1 for $12 < Z < 30$ and does not overcome ± 2 for $Z > 30$. We consider these values as representative of the uncertainties concerning the *AME* method itself for the determination of the atomic mass A. In the following, we are going on to evaluate the *AME* method by looking to more direct experimental quantities.

4.2. Experimental checks

The isotopic identification can be further qualified by some specific tests made directly with the help of experimental data. As a first stage, we can provide a quite accurate estimate for the mass number A even if the full isotopic resolution is not achieved. We remind that, knowing the thickness of the Silicon detector (300 μm all along this section), the atomic number Z value of a detected fragment and the well determined ΔE, corrected for the PHD [38,39], we can start by proposing an atomic mass A_i number and compute the corresponding residual energy E_{0i} in the CsI stage using the energy loss tables. They are connected to the calculated scintillation light $\mathcal{L}_i = \mathcal{L}(E_{0i}, A_i)$ via the Eq. (3). Then, the integer mass number is varied, by steps of one unit, in order to minimize the quantity $d_i = |\mathcal{L}_i - \mathcal{L}_{exp}|/\mathcal{L}_{exp}$, in such a way that the measured ΔE value be reproduced too. After a few iterations, the best integer value A^* of A_i and the related value of E_{0i} are found, characterized by the shortest normalized distance d_i between the calculated $\mathcal{L}_i$ and experimental $\mathcal{L}_{exp}$ light. Finally, to get a representative value A_{est} for the estimated mass number in a single event (one experimental point in the $\Delta E - \mathcal{L}$ plot) at a given ΔE, we simply weight the different A_i values by the inverse of d_i^2 as:

$$A_{est} = \frac{1}{\Sigma_i \frac{1}{d_i^2}} \Sigma_i \frac{A_i}{d_i^2} \tag{4}$$

Thus, we shall exploit not only the mass number as an integer but directly the PID, defined above as: $PID = 8Z + A_{est}$, by letting now the mass number A_{est} to be a *real* number. Of course, for an experimental light $\mathcal{L}_{exp}$, the main contributions to A_{est} are coming from the shortest distances d_i. Doing so, we can obtain an estimation concerning the uncertainty δA by taking the absolute difference between the optimum value A^*, corresponding to the smallest distance d_i and the weighted value A_{est} obtained with the Eq. (4):

$$\delta A = |A^* - A_{est}| \tag{5}$$

If the two values A_{est} and A^* are close enough ($\delta A < 0.5$, so comprised in one unit range), we assume a full isotopic identification, whereas if $\delta A \geq 0.5$, we have only a limited isotopic identification. This procedure can be therefore considered as a simple and easy way to qualify the isotopic identification. This is illustrated by the black and grey/red numbers on Figs. 4 and 5. The black numbers refer to $\delta A < 0.5$ whereas the grey/red ones to $\delta A \geq 0.5$.

In order to further evaluate the validity of the method, we have also used *INDRA* results for the four different systems: ^{124,136}Xe + ^{112,124}Sn

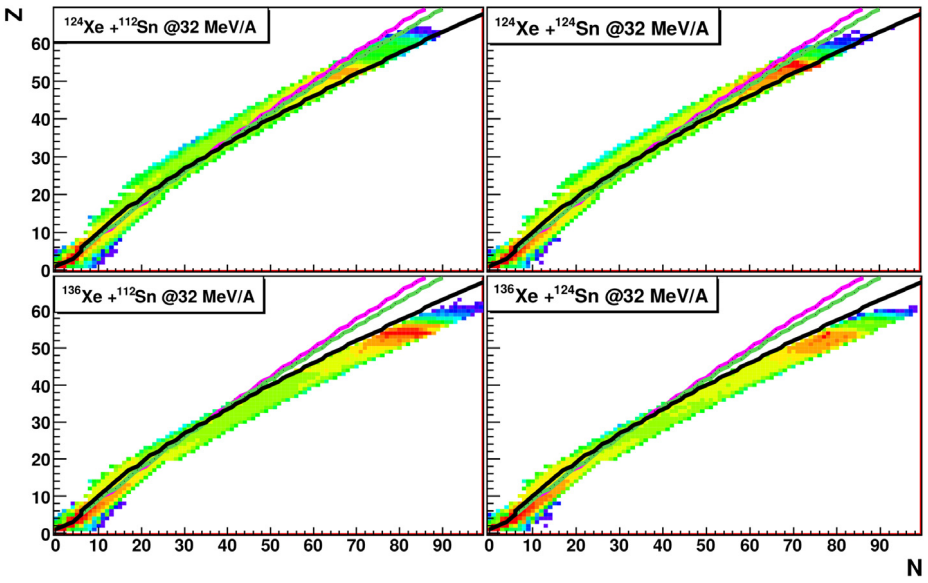

Fig. 12. $Z-N$ charts of the detected nuclei in the forward rings (1–9) of *INDRA* for a trigger multiplicity $M \geq 4$ from the four reactions ^{136,124}Xe + ^{112,124}Sn at 32A MeV. Data correspond to the *AME* method. The different grey/coloured curves correspond to the EAL hypotheses on the neutron number N and the black line to the β-stability valley one. See text for explanation. (colour online).

at 32 AMeV. Several tests are then proposed in the following. First, we have looked to data at the most forward angles, from rings 1–5, *i.e.* $2° \leq \theta \leq 15°$. These ones are obtained from the system ^{136}Xe + ^{112}Sn at 32 AMeV, by requiring a trigger multiplicity (fired telescopes) $M \geq 1$, in order to select mostly quasi-elastic events. From Fig. 3, we could indeed notice that we recover as main contribution the quasi-projectile ($Z \approx 54$) in the most forward rings. For such high Z values, the isotopes are not visually separated in the $\Delta E - \mathcal{L}$ matrix; in the framework of the standard method, a hypothesis on the mass has to be made for finding their velocities starting from the measured energies deposited in the 1st stage of a telescope. Fig. 9 displays the correlation between the mass and the velocity parallel to the beam, for different ejectiles and for different mass estimates. The yellow stars indicate the maximum number of entries.

The two upper panels of Fig. 9 display the $A - V_z$ correlation for the standard case (usual $\Delta E - E$ type), where only the atomic number Z is determined from the $\Delta E - \mathcal{L}$ plot. In the upper panel, for $Z = 54$ we took as mass hypothesis the prediction $A = 120$ for the Evaporation Attractor Line (EAL) [41] (see below). It leads to a value $V_z \approx 8.5$ cm/ns of velocity parallel to the beam direction. In the middle panel, the β-stability hypothesis is used, and the mass for xenon is set to $A = 129$, richer in neutron, and results $V_z \approx 8.2$ cm/ns. In both cases, the values of the atomic mass A and the parallel velocity are peaked quite far from the expected elastic contribution, in the present case: $A = 136$ and $V_z = 7.9$ cm/ns represented by the filled circles on Fig. 9. This is due to the incorrect attributed values of the mass number A, simply calculated from the atomic numbers Z via different hypotheses. Consequently, the corresponding parallel velocities V_z are also incorrect since they were computed by means of these hypothetical A values. At variance, we can notice that applying the iterative AME method – lower panel of Fig. 9 –, the plotted distribution presents at $A \approx 133$ and $V_z \approx 8.0$ cm/ns a maximum located much closer to the elastic contribution. We could therefore infer that the obtained results with AME are more valid for the (n)-rich projectiles even for these very heavy ions detected in the region of quasi-elastic events. We also found the same conclusion for the proton (p)-rich system ^{124}Xe + ^{112}Sn at 32A MeV.

Now, if we look at the PID distributions in Fig. 10, we may stress also the differences. In the upper panel, when we are not using the scintillation light to determine the mass number (usual method), we can get some partial isotopic identification up to Z = 6–8. By contrast, as shown in the lower panel, thanks to the new *AME* method, we are now able to distinguish a fair isotopic identification up to at least $Z \approx 12$–13 for which we have $\delta A \leq 0.5$ as obtained from Eq. (5) for the most abundant isotopes; this latter is fully consistent with the sensitivity analysis presented in the previous section. The improvement concerning the isotopic resolution is indeed obtained by taking into account the supplemental information of the light from the CsI crystal.

We could also qualify the accuracy of the isotopic identification for Z much higher than 12 by taking advantage once again of the elastic channel for both reactions. For a trigger multiplicity $M = 1$, an angular range between 2° and 7° (rings 1–3), and by selecting only the xenon nuclei ($Z = 54$), we obtain the isotopic distributions displayed in Fig. 11. These latters are centred around $A \approx 124$ for ^{124}Xe (the mass of the projectile) and $A \approx 133$ for ^{136}Xe (three mass units smaller than the projectile). For the ^{136}Xe data, due to its neutron richness, one could expect a loss of few neutrons for the projectile even in very peripheral collisions, transforming thus the elastic contribution into a quasi-elastic one. The results are therefore compatible with physical arguments and with those shown in the lower panel of Fig. 9 (mass–velocity correlation). The width of these isotopic distributions reflect indeed the convolution of the physical isotopic distribution as well as the uncertainty on the determined mass. We can therefore reasonably deduce that the difference of 3 mass units found in Fig. 11 could represent an *upper* limit for the mass uncertainty.

Finally, we display in Fig. 12 the $N - Z$ charts for the reaction products in the above-mentioned reactions, their masses being determined via the *AME* procedure. We have selected the trigger condition $M \geq 4$, thus removing the major part of the quasi-elastic contribution presented in the previous Figs. 9,11. The grey/coloured curves represent the evaporation attractor lines [41], predicting the number of neutrons N as an integer function of Z: the steeper/pink line, with $N = 1.072Z + 2.032 \times 10^{-3}Z^2$ recommended for $Z < 50$ and the more gentle slope/green line, with $N = 1.045Z + 3.57 \times 10^{-3}Z^2$ recommended for $Z \geq 50$. The black curve indicates a 3rd degree polynomial fit of the β-stability valley as the integer of $N = 1.2875 + 0.7622Z + 1.3879 \times 10^{-2}Z^2 - 5.4875 \times 10^{-5}Z^3$, with *i.e.* nuclei more (n)-rich than for the EAL lines.

The $Z - N$ charts in Fig. 12 concern the forward detection angles: $2° \leq \theta \leq 45°$(rings 1–9 of *INDRA*). These data seem to reflect mainly the ratio N/Z of the projectile and none of these hypotheses on the number N of neutrons, and consequently on A, is able to reproduce in average the results, especially for the (n)-rich ^{136}Xe projectiles (lower panels). This overall view pleads in favour of the *AME* procedure compared to a

simple mass hypothesis. With the present method we can obtain a better calibration of very thick CsI(*Tl*) scintillators allowing at the same time the full detection of very energetic charged reaction products and their mass determination with the best resolution. *AME* upgrades thus the 4π *INDRA* array, designed to measure only the atomic number Z of the heavy nuclear fragments stemming from multifragmentation reactions, to a device able to estimate their mass A too, up to $Z \approx 12$–13 for an isotopic resolution $\delta A \leq 0.5$ and $Z \approx 54$ for $\delta A \leq 3$, and this in a very compact geometry.

5. Conclusion

We have presented a method called Advanced Mass Estimate (*AME*), a new approach for isotopic identification in Si–CsI telescopes using the analytical formulation for the CsI(*Tl*) light response provided in [33]. It includes explicitly the light quenching and the δ-rays contribution to the scintillation of the CsI(*Tl*) crystals. In this framework, we have shown that it is possible to use an iterative procedure to accurately calibrate the CsI detectors and, at the same time, to estimate the mass number A of the charged reaction products, besides the atomic number Z, with a resolution better than the one previously achieved by standard techniques. This method allows to recover not only the isotopic distributions obtained by the usual visual techniques for $Z = 1$–8, but it can also be extended safely up to $Z \approx 12$–13, and with an uncertainty of plus or minus one atomic mass unit for higher atomic numbers (< 30) for the telescopes of the *INDRA* array. In addition, from the comparison with experimental data, we have shown that it is reasonably possible to estimate the atomic mass within 3 mass units up to xenon isotopes, if one is able to carefully evaluate the thickness and the pulse height defect in the ΔE silicon layer. We then consider that the quality of *INDRA* Si–CsI experimental results can be dramatically improved by using the new *AME* method, and that is particularly well adapted to undergo analyses with radioactive beams exploring a large N/Z domain. The *AME* method is not only suited for *INDRA* Si–CsI(Tl) telescopes but can be also successfully exploited with any charged particle array using the same kind of telescopes. Further studies concerning the implementation of the Recombination and Nuclear Quenching Model with the exact treatment mentioned in the first section are currently in progress, by using high-quality data from *FAZIA* telescopes, and will be the subject of a forthcoming paper.

References

[1] B.A. Li, A. Ramos, G. Verde, I. Vidana, Topical issue on nuclear symmetry energy, Eur. Phys. J. A 50 (2) (2014) and references therein.

[2] F. Gulminelli, W. Trautmann, S.J. Yennello, Ph. Chomaz, Dynamics and thermodynamics with nuclear degrees of freedom, Eur. Phys. J. A 30 (1) (2006) and references therein.

[3] R.D. Evans, The Atomic Nucleus, McGraw-Hill Book Company, 1955;
H.A. Enge, Introduction Tu Nuclear Physics, second ed., Addison - Wesley Publishing Company, 1969;
G.F. Knoll, Radiation Detection and Measurement, fourth ed., J. Wiley and Sons Inc., 2010 references therein.

[4] F.W. Aston, Phil. Mag. (London) 38 (1919) 707.
J. Mattauch, Phys. Rev. 50 (1936) 617;
K. Siegbahn, Physica 18 (1952) 1043;
H.A. Enge, Rev. Sci. Instr. 29 (1958) 885 and 34 (1963) 155.

[5] J. Rainwater, W.W. Havens Jr., Phys. Rev. 70 (1946) 136 and 154;
E. Melkonian, Phys. Rev. 76 (1949) 1750;
F. Ajzenberg, Phys. Rev. 88 (1952) 298 and 124 (1961) 1548.

[6] D.A. Bromley, IRE Trans. Nucl. Sci. NS-9 (3) (1962) 135;
F.S. Goulding, B.G. Harvey, Ann. Rev. Nucl. Sci. 25 (1975) 167;
D.G. Berry, L.P. Remsberg, Nucl. Instrum. Methods 135 (1976) 103.

[7] L.M. Bollinger, G.E. Thomas, Rev. Sci. Instr. 32 (1961) 1044;
M.L. Roush, et al., Nucl. Instrum. Methods 31 (1964) 112 and references therein.

[8] L. Varga, Nucl. Instrum. Methods 14 (1961-1962) 24 and references therein.

[9] A.G. Seamster, et al., Nucl. Instrum. Methods 145 (1977) 583.

[10] R.T. de Souza, et al., Eur. Phys. J. A 30 (2006) 275.

[11] H.A. Enge, Nucl. Instrum. Methods 186 (1981) 413 and references therein;
S. Pullanhiotan, M. Rejmund, et al., Nucl. Instrum. Methods Phys. Res. A 593 (2008) 343; Nucl. Instrum. Methods Phys. Res. B 266 (2008) 4148;
C. Schmitt, M. Rejmund, et al., Nucl. Instrum. Methods Phys. Res. A 621 (2010) 558 and 646 (2011) 184 and references therein.

[12] F. Cappuzzello, et al., Nucl. Instrum. Methods Phys. Res. A 621 (2010) 419;
T. Kobayashi, et al., Nucl. Instrum. Methods Phys. Res. B 317 (2013) 294 and 739;
Nucl. Instrum. Methods Phys. Res. B 376 (2016) 175;
M. Aguilar, et al., Phys. Rev. 110 (2013) 141102 and references therein.

[13] Th. Blaich, et al., Nucl. Instrum. Methods Phys. Res. A 314 (1992) 136;
A. Gobbi, et al., Nucl. Instrum. Methods Phys. Res. A 324 (1993) 156;
I. Tilquin, Y. El Masri, M. Parlog, et al., Nucl. Instrum. Methods Phys. Res. A 365 (1995) 446;
A. Buta, et al., Nucl. Instrum. Methods Phys. Res. A 455 (2000) 412.

[14] M.C.S. Williams, J. Phys. G: Nucl. Part. Phys. 39 (2012) 123001;
C. Lippmann, Nucl. Instrum. Methods Phys. Res. A 666 (2012) 148;
T. Nakamura, Y. Kondo, Nucl. Instrum. Methods Phys. Res. B 376 (2016) 156.

[15] R. Bougault, et al., Nucl. Instrum. Methods Phys. Res. A 259 (1987) 473;
R.T. de Souza, et al., Nucl. Instrum. Methods Phys. Res. A 295 (1990) 109;
S. Aiello, et al., Nucl. Instrum. Methods Phys. Res. A 369 (1996) 50 and A 400 (1997) 469 and references therein.

[16] M. Alderighi, et al., Nucl. Instrum. Methods Phys. Res. A 489 (2002) 257;
F. Gramegna, et al., Nucl. Instrum. Methods Phys. Res. A 389 (1997) 474;
S. Wuenschel, Nucl. Instrum. Methods Phys. Res. A 604 (2009) 578.

[17] The FAIR collaboration, FAIR CDR - An International Accelerator Facility for Beams of Ions and Antiprotons, Conceptual Design Report, Technical Report, GSI, 2001; T. Aumann, B. Jonson, Technical Proposal for the Design, Construction, Commissioning and Operation of R3B - A Universal Setup for Kinematical Complete Measurements of Reactions with Relativistic Radioactive Beams, Technical Report, The R3B Collaboration, 2005.

[18] B. Pietras, Nucl. Instrum. Methods Phys. Res. A 729 (2013) 77;
M. Gascon, et al., JINST 8 (2013) P10004;
Alvarez-Pol, et al., Nucl. Instrum. Methods Phys. Res. A 767 (2014) 453.

[19] R. Bougault, et al. (FAZIA collaboration), Eur. Phys. J. A 50 (2014) 47.

[20] S. Carboni, et al. (FAZIA collaboration), Nucl. Instrum. Methods Phys. Res. A 664 (2012) 251.

[21] P.F. Mastinu, et al., Nucl. Instrum. Methods Phys. Res. A 371 (1996) 510.

[22] M. Alderighi, et al., Comput. Phys. Comm. 140 (2001) 13.

[23] L. Tassan-Got, Nucl. Instrum. Methods Phys. Res. B 194 (2002) 503.

[24] N. Le Neindre, et al., Nucl. Instrum. Methods Phys. Res. A 490 (2002) 251.

[25] A. Pagano, et al., Nuclear Phys. A 681 (2001) 331c.

[26] J. Pouthas, et al., Nucl. Instrum. Methods Phys. Res. A 357 (1995) 418.

[27] H.A. Bethe, Ann. Phys. 5 (1930) 325.

[28] J.F. Ziegler, Handbook of Stopping Cross Sections for Energetic Ions in All Elements, in: Stopping and Ranges of Ions in Matter, vol. 5, Pergamon Press, New York, 1980.

[29] J. Lindhard, M. Scharff, H.E. Schiott, K. Dan Vidensk, Selk. Mat. Fys. Medd. 33 (14) (1963) 1–42.

[30] L.C. Northcliffe, R.F. Schilling, Nucl. Data Tables A7 (1970) 233.

[31] F. Hubert, R. Bimbot, H. Gauvin, At. Data Nucl. Data Tables 46 (1990) 1.

[32] M. Parlog, et al., Nucl. Instrum. Methods Phys. Res. A 482 (2002) 674.

[33] M. Parlog, et al., Nucl. Instrum. Methods Phys. Res. A 482 (2002) 693.

[34] J.B. Birks, The Theory and Practice of Scintillation Counters, Pergamon Press, Oxford, 1964.

[35] D. Horn, et al., Nucl. Instrum. Methods Phys. Res. A 320 (1992) 273.

[36] E. De Filippo, et al., Nucl. Instrum. Methods Phys. Res. A 342 (1994) 527.

[37] A. Meyer, R.B. Murray, Phys. Rev. 118 (1962) 98.

[38] G. Tabacaru, et al., Nucl. Instrum. Methods Phys. Res. A 428 (1999) 379.

[39] J.B. Moulton, J.E. Stephenson, R.P. Schmitt, G.J. Wozniak, Nucl. Instrum. Methods 157 (1978) 325.

[40] G. Ademard, et al. (INDRA collaboration), Eur. Phys. J. A 50 (2014) 33.

[41] R.J. Charity, Phys. Rev. C 58 (1998) 1073.